Accurate intravoxel incoherent motion parameter estimation using Bayesian fitting and reduced number of low b-values

Chen Ye, Daoyun Xu, Yongbin Qin, Lihui Wang, Rongpin Wang, Wuchao Li, Zixiang Kuai, Yuemin Zhu

Accurate Intravoxel Incoherent Motion Parameter Estimation Using Bayesian Fitting and Reduced Number of Low b-Values

Chen Ye[1], Daoyun Xu[1]*, Yongbin Qin[1], Lihui Wang[1], Rongpin Wang[2], Wuchao Li[2], Zixiang Kuai[3] and Yuemin Zhu[4]

[1]Key Laboratory of Intelligent Medical Image Analysis and Precise Diagnosis of Guizhou Province, School of Computer Science and Technology, Guizhou University, Guiyang, China.

[2]Department of Radiology, Guizhou Provincial People's Hospital, Guiyang, China

[3]Harbin Medical University Cancer Hospital, Harbin, China

[4]Univ Lyon, INSA Lyon, CNRS, INSERM, CREATIS UMR 5220, U1206, F-69621, Lyon, France

Running title: IVIM parameter mapping of brain tumors

*Correspondence: Daoyun Xu, Ph.D.

Address : College of Computer Science and Technology, University of Guizhou, Huaxi District, Guiyang, China 550025.

Email: dyxu@gzu.edu.cn

Abstract

Purpose: Intravoxel incoherent motion (IVIM) magnetic resonance imaging is a potential non-invasive technique for the diagnosis of brain tumors. However, perfusion-related parameter mapping is a persistent problem. The purpose of this paper is to investigate the IVIM parameter mapping of brain tumors using Bayesian fitting and low b-values.

Methods: Bayesian shrinkage prior (BSP) fitting method and different low b-value distributions were used to estimate IVIM parameters (diffusion *D*, pseudo-diffusion *D**, perfusion fraction *F*). The results were compared to those obtained by least-squares (LSQ) on both simulated and in vivo brain data. Relative error (RE) and reproducibility were used to evaluate the results. The differences of IVIM parameters between brain tumor and normal regions were compared and used to assess the performance of Bayesian fitting in the IVIM application of brain tumor.

Results: In tumor regions, the value of *D** tended to be decreased when the number of low b-values was insufficient, especially with LSQ. BSP required less low b-values than LSQ for the correct estimation of perfusion parameters of brain tumors. The IVIM parameter maps of brain tumors yielded by BSP had smaller variability, lower RE and higher reproducibility with respect to those obtained by LSQ. Obvious differences were observed between tumor and normal regions in parameters *D* ($p<0.05$) and *F* ($p<0.001$), especially *F*. BSP generated fewer outliers than LSQ, and distinguished better tumors from normal regions in parameter *F*.

Conclusions: IVIM parameters clearly allow brain tumors to be differentiated from normal regions. Bayesian fitting yields robust IVIM parameter mapping with fewer outliers and requires less low b-values than LSQ for the parameter estimation.

Keywords: IVIM; Bayesian shrinkage prior; low b-values; least squares; brain tumor; perfusion.

1. Introduction

Intravoxel incoherent motion (IVIM) magnetic resonance imaging technique, initially introduced by Le Bihan et al.[1], aims to separate water molecule diffusion (*D*) component and microvascular perfusion or pseudo-diffusion (*D**) component in the diffusion-weighted (DW) signals of tissues. By simplicity, in what follows, "perfusion" and "pseudo-diffusion" will be used interchangeably. Perfusion-related information (pseudo-diffusion *D**, perfusion fraction *F*) was shown to be able to

diagnose brain tumors, such as tumor grading [2–5] and differentiation of recurrent tumors from post-treatment effects.[6, 7]

However, reliable estimation of perfusion-related parameters is a persistent problem.[4, 8–12] The most common approach to obtaining IVIM parameter maps is the nonlinear least squares (LSQ) method based on the Levenberg-Marquardt algorithm or similar ones.[7, 13–17]The LSQ method consists in estimating the parameters by solving a regression problem, namely by minimizing the residual between actual and fitted DW signals. Because of the nonlinear structure of IVIM model, one can only obtain the solution of the objective function in an approximate way. To cope with this problem, many researchers approximated the nonlinear DW signal attenuation by a log-linear model and only diffusion D was taken as the decay rate parameter.[13, 18] However, such modified model does not take into account the independent characterization of diffusion and perfusion components.[18]

To improve the robustness of LSQ fitting, an alternative approach, called the segmented least squares fitting,[7, 13–16] is used. The method assumes that the impact of D^* on DW signals can be neglected at high b-values (> 200 s/mm^2). It consists of first fitting the diffusion parameter D (and S_0 that is used to estimate F) using a mono-exponential model, then calculating the perfusion fraction F with the fitted S_0 signal, and finally estimating the pseudo-diffusion parameter D^* using nonlinear least squares fitting. However, estimating the parameters using such approach causes bias errors due to the assumption on the influence of D^* at high b-values.

All the limitations mentioned above are due to LSQ fitting itself. More recently, Bayesian methods have been proposed to solve the regression problem in a probabilistic manner. Bayesian methods estimate IVIM parameters by maximizing a posterior probability of IVIM parameters given the observed signal. [18–21]Freiman et al. obtained the improved IVIM parameter mapping using Bayesian spatial homogeneity prior (FBM).[18] Orton et al. tried to reduce the outlying estimation by using Bayesian Gaussian shrinkage prior (BSP).[19] However, solving the regression problem using the Bayesian methods also has some limitations, such as the dependence on tissue heterogeneity. So far, Bayesian methods were mainly applied to organs such as liver[18, 19] and heart.[20]

Meanwhile, b-value being an imaging parameter that reflects the measurement sensitivity to diffusion related to the strength and duration of diffusion gradients, the estimation of D^* is often affected by the number of low b-values (b< 50 s/mm^2), especially for organs having high pseudo-diffusion coefficients, such as liver [22–25] and kidney.[26] It is generally recognized that brain is a

low-perfusion tissue. However, previously reported studies showed that hyper perfusion was found in brain tumor regions, in terms of F [2, 3, 5, 10, 11, 27, 28] and D*. [4] Therefore, further study of the effect of low b-values on the perfusion-related parameters of brain tumors appears interesting and necessary.

The present work aims to investigate the IVIM parameter mapping of brain tumors using Bayesian fitting and low b-values. To this end, BSP fitting method and different low b-value distributions were used to estimate IVIM parameters (D, D* and F). The results were compared to those obtained by LSQ fitting on both simulated and in vivo data.

2. Materials and Methods

2.1. Simulation

In order to evaluate the joint effect of low b-values and Bayesian fitting on IVIM parameter estimation, we used a bi-exponential model with noise [19] to simulate IVIM signals,

$$S_n = S_0(Fe^{-b_n D^*} + (1-F)e^{-b_n D}) + \varepsilon_n, \quad (1)$$

where S_n is the signal measured at the b-value b_n, S_0 the signal with no diffusion weighting, F the perfusion flow fraction, D^* the pseudo-diffusion coefficient, D the diffusion coefficient, and ε_n the additive noise.

In the simulation, to investigate the effect of low b-values, various b-value configurations with different number of low b-values (0<b<50 s/mm^2) were used: with four low b-values (0, 10, 20, 30, 40, 50, 70, 100, 200, 400, 600, 800, 1000 s/mm^2), with three low b-values (0, 20, 30, 40, 50, 70, 100, 200, 400, 600, 800, 1000 s/mm^2), with two low b-values (0, 30, 40, 50, 70, 100, 200, 400, 600, 800, 1000 s/mm^2), with 1 low b-value (0, 40, 50, 70, 100, 200, 400, 600, 800, 1000 s/mm^2), and without low b-value (0, 50, 70, 100, 200, 400, 600, 800, 1000 s/mm^2). Considering the influence of noise, Gaussian noise was added to signals with four different signal-to-noise ratios (SNRs): 20, 40, 60, and 80. The SNR was calculated as the ratio of mean signal intensity to standard deviation of noise intensity on b0 image.[14, 29]Meanwhile, since noise models may impact the performance of fitting methods, Rician noise model was also considered by adding complex Gaussian noise to each signal and calculating the magnitude. The different SNRs were: 2, 10, 20, and 80. For the simulations, the tumor regions of in vivo brain images were selected and the corresponding IVIM parameters at each voxel of the tumor region

were estimated by LSQ method. The so obtained parameters D^*, D and F were then used as the ground-truth for the simulation. Considering that low b-values for different perfusion regions have different effects on parameter estimation, two different sets of data with different mean pseudo-diffusion coefficients (high/low, 45.8/6.9 x 10^{-3} mm^2/s) were simulated.

Using Eq. (1) and the simulation parameters mentioned above, realistic DW images were simulated and subsequent IVIM parameters were estimated from the simulated DW images with Gaussian noise using LSQ and BSP fitting methods respectively. After that, a quantitative analysis is performed by comparing the estimated IVIM parameters and the ground-truth. Furthermore, the parameter estimation performance of BSP method with different noise models and different number of low b-values was evaluated on simulated DW images with Rician noise.

On the other hand, since the performance of LSQ or BSP may be affected by the heterogeneity of IVIM parameters in ROI, LSQ and BSP were investigated on heterogeneous regions. To do this, a ROI of a healthy brain was first selected. Then, if IVIM parameter maps calculated using LSQ on the ROI were heterogeneous, the estimated parameters at each voxel of the ROI were used as the ground-truth for the simulation. Rician noise was considered by adding complex Gaussian noise to each signal and calculating the magnitude,[13, 30] for different SNRs (20, 40, 60, 80). Finally, BSP and LSQ were performed on the ROI using different number of low b-values.

Finally, investigations on homogeneous regions were also performed. The IVIM parameters for the simulation were set according to previous studies on brain[4]: D (high/low)=2.69/0.71 x 10^{-3} mm^2/s, D^* (high/low)=49/5.81 x 10^{-3} mm^2/s, F (high/low)=0.18/0.1. The simulated region was an 80 x 80 matrix containing eight (corresponding to eight combinations because there are three IVIM parameters, each of them has two values high and low) rectangular subregions of equal size. In each subregion (rectangle), the IVIM parameter value was set as a constant (high or low). The parameter value of the intermediate regions outside the eight subregions was set to the average of high and low values. In this way, different homogeneous regions were obtained (Fig. 6). Rician noise was added to signals with different SNRs: 20, 40, 60 and 80. After that, BSP and LSQ were performed on these homogenous regions using different number of low b-values.

2.2. DW image acquisitions

The present work was approved by the local Ethics Committee. Informed consent was obtained from each patient. DWI data of eight (four tumor and four normal) human brains were acquired with 3.0 Tesla MRI scanner (GE Discovery MR750). The acquisition protocol is as follows: echo planar imaging (EPI) sequence; 256x256 mm field of view; 128x128 matrix; 5 mm slice thickness; TE/TR=77/2800 ms; b-values are 0, 10, 20, 30, 40, 50, 70, 100, 200,400, 600, 800 and 1000 s/mm^2; diffusion gradient was in three orthogonal directions and trace-weighting was applied. Four tumor ROIs and the corresponding four normal ROIs from different subjects were selected for the analysis. To reduce the influence of noise, DW scanning of the same brain was repeated 2 times and the scans were then averaged to improve the SNR [29, 31]. The SNRs of in vivo brains at the highest b-value ranged from 25.41 to 38.78, and the averaged SNR is 34.74. The SNR was calculated as the ratio of the mean signal of b1000 image (the highest b-value) to the standard deviation of noise. The noise was estimated from background region that did not present contaminations by ghosting or flow artifacts.[32]

In order to study the effect of low b-values, different number of low b-values were used in the fitting process, which are the same as those used in the simulation described above.

2.3. Estimation of IVIM parameters.

2.3.1. Least Squares Fitting

The LSQ method implemented in the present study is the commonly used one in practical applications. It consists in estimating the IVIM parameters by minimizing the difference between predicted and original signals:

$$\min \sum_{n=0}^{N} (S_n - S_n^{'})^2 , \quad (2)$$

where S_n is the original signal, and $S_n^{'}$ the predicted signal fitted by LSQ.

In the present work, considering that the brain is a low-perfusion tissue, the segmented LSQ method may lead to bias error; we therefore used the traditional LSQ method to evaluate the parameters in a whole process. The initial values of D and F for LSQ estimation were chosen according to the results given by the segmented LSQ, and D^* was set as the common value (D^*=20 x 10^{-3} mm^2/s) of brain according to previous studies.[4]

In order to improve the robustness of fitting, constraints on IVIM parameters were used as in [19]: $0.0005 \le F \le 0.9995$; $0.0045 \le D \le 18$ (x 10^{-3} mm^2/s); $0.034 \le D^* \le 1000$ (x 10^{-3} mm^2/s).

2.3.2. Bayesian Shrinkage Prior Inference

The BSP method is based on using Gaussian shrinkage prior. The fitting process aims to maximize a joint posterior probability and is realized by using a Markov chain Monte Carlo (MCMC) method. The Bayesian modeling process is described as follows.[19]

Using the IVIM model of Eq. (1), the data Gaussian likelihood reads:

$$p(S \mid F, D, D^*, S_0, \sigma_s^2) = (2\pi\sigma_s^2)^{-N/2} \exp\left(-\frac{1}{2\sigma_s^2} \sum_{n=1}^{N} (S_n - S_0 g_n)^2 \right), \quad (3)$$

where $S = [S_1, S_2 \cdots S_N]^T$, $g_n = Fe^{-b_n D^*} + (1-F)e^{-b_n D}$, σ_s^2 is the variance of the error term ε_n in Eq. (1) with Gaussian distribution, and N is the number of b-values.

In this model, the parameters S_0 and σ_s^2 were marginalized out, as described by Orton et al., and the marginalized Gaussian likelihood can be written as:

$$p(S \mid F, D, D^*) \propto [S^T S - (S^T g)^2 / (g^T g)]^{-N/2} . \quad (4)$$

where $g=[g_1\ g_2\ .\ .\ .\ g_n]^T$ is a vector containing the expected signal g_n at the n^{th} b-value.

The shrinkage prior is assumed to be a multivariate Gauss distribution and can be represented as:

$$p(\theta_i \mid \mu, \Sigma_\mu) = \mid 2\pi\Sigma_\mu \mid^{-1/2} \exp(-\frac{1}{2}(\theta_i - \mu)^T \Sigma_\mu^{-1} (\theta_i - \mu)) , \quad (5)$$

where $\theta = (f, d, d^*)$ is a vector including the transformed IVIM parameters: $f = \ln(F) - \ln(1-F)$, $d = \ln D$ and $d^* = \ln D^*$. $\mu = (\mu_f, \mu_d, \mu_{d^*})$ is a vector containing the mean values of the transformed parameter in ROI, Σ_μ is the corresponding covariance matrix, and *i* denotes the current pixel.

Given the observed data, the posterior probability of IVIM parameters estimated at each pixel can be expressed as:

$$p(\theta_{1:M}, \mu, \Sigma_\mu \mid S_{1:M}) \propto \prod_{i=1}^{M} p(S_i \mid \theta_i)\, p(\theta_i \mid \mu, \Sigma_\mu) , \quad (6)$$

where $\theta_{1:M} = [\theta_1, \theta_2, \cdots, \theta_M]$, $S_{1:M} = [S_1, S_2, \cdots, S_M]$, and M is the number of pixels.

The iterative fitting process was realized by MCMC algorithm as illustrated in Fig. 1.

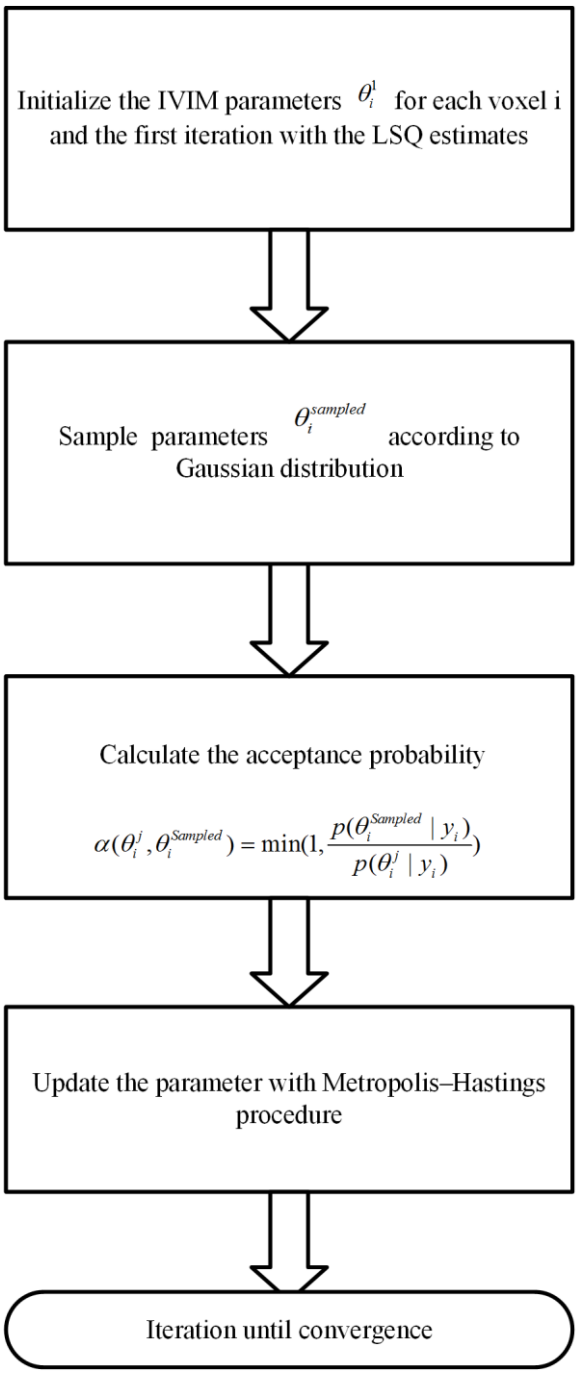

Fig. 1 Flowchart of BSP fitting.

In addition, the additive noise ε_n in Eq. (1) is often assumed to be Gaussian due to the fact that noise in MRI is nearly governed by Gaussian distribution when SNR>2.[33] Rician distribution noise is however considered when magnitude data is used and SNR is low.[21, 33] The likelihood function based on Rician noise can be expressed as:

$$p(S \mid F, D, D^*, S_0, \sigma_s^2) = \frac{S_n}{\sigma_s^2} \exp\left(-\frac{1}{2\sigma_s^2} (S_n^{\,2} + S^{'}(b_n)^2) \right) I_0\left(\frac{S_n S^{'}(b_n)}{\sigma_s^2}\right) \quad (7)$$

where S_n is the measured signal at b_n, $S'(b_n)$ the expected signal at b_n and σ_s^2 the variance of ε_n with Rician distribution. I_0 is the modified zeroth-order Bessel function of the first kind.[33]

When larger b-values are used (b>1000 s/mm^2), Rician noise is likely to be evident due to the low SNR.[32] However, Rician distribution tends toward Gaussian distribution at higher SNRs.[32, 33] Since, as mentioned above, temporal averaging was performed in the present study to improve the SNR of in vivo data and the averaged SNR at the highest b-value (b=1000 s/mm^2) was 34.74, that guarantees Gaussian characteristic of the noise. With the Rician model, the marginalized Gaussian likelihood in Eq. (4) is no longer valid. Instead, σ_s^2 should be estimated (estimated from background noise) and S_0 should also be estimated during the subsequent parameter estimation process.

2.4. Quantitative Evaluation

The effect of Bayesian fitting and low b-values on IVIM parameter mapping was evaluated using several criteria. For simulation results, relative error (RE) for IVIM parameters was calculated at each voxel as follow:

$$\mathrm{RE}_{\mathrm{i:n}} = \frac{|(G_i - P_i)|}{G_i} \times 100\,, \tag{8}$$

where G_i is the ground-truth, P_i is the predicted IVIM parameters, and i represents the i^{th} pixel.

The mean values of the parameters estimated with different number of low b-values in the tumor ROI were compared in both simulations and in vivo experiments. Bland-Altman analysis was performed to evaluate the intra-subject reproducibility of two consecutive brain scans. The differences in IVIM parameters between brain tumor and normal ROIs were compared. Finally, statistical significance of differences in parameters between brain tumor and normal ROIs and RE between the fitting methods was tested using two-sample t-test and the fitting methods were implemented in Matlab.

The average fitting time for LSQ and BSP is 3 x 10^{-2} s/ voxel and 4 x 10^{-1} s/voxel, respectively. All the calculations were performed on a laptop (Inter(R) Core(TM) i7-5500U CPU, 2.40GHz).

3. Results

3.1. Simulated images

Two simulations with different pseudo-diffusion coefficients and Gaussian noise were performed with different b-value configurations. To show visually the difference between estimated parameters and ground-truth, in Fig. 2 are given the RE maps. Obviously, in the high-perfusion region (Fig. 2(a)), the REs generated by BSP are lower than those produced by LSQ for the three IVIM parameters ($p<0.001$). When reducing the number of low b-values, the RE of D^* increases, especially with the use of LSQ. However, the estimation of D or F is insensitive to the number of low b-values. The REs in low-perfusion regions are shown in Fig. 2(b). Similarly to Fig. 2(a), BSP results in lower error than LSQ, but the influence of low b-values on D^* estimation was reduced.

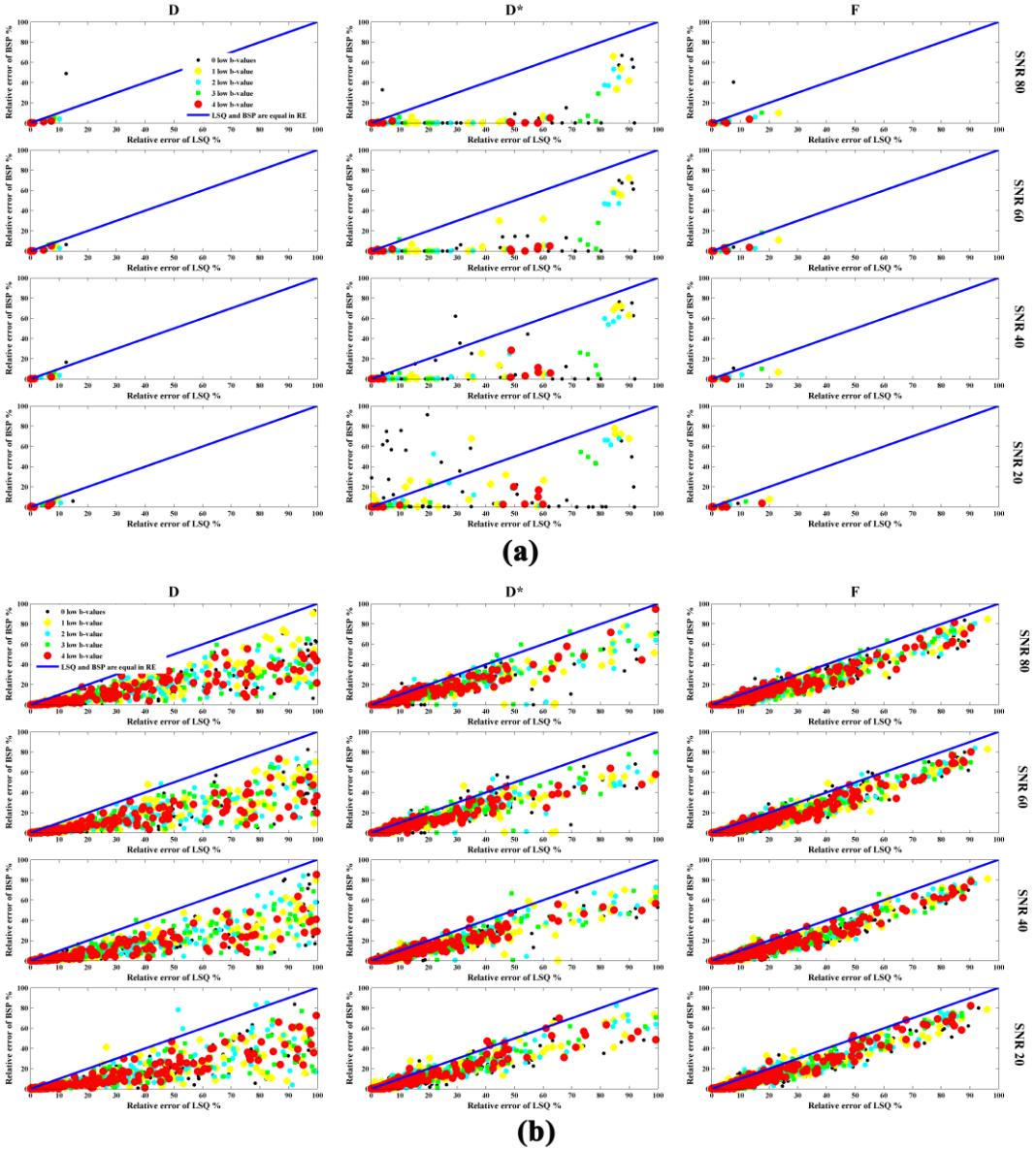

Fig. 2. Relative errors (REs) of the estimated IVIM parameters on simulation data with Gaussian noise. (a) REs in high-perfusion region (b) REs in low-perfusion region. The coordinates of each point represent the RE of each voxel obtained using the two fitting methods.

To further analyze the influence of low b-values on the estimation of IVIM parameters, we summarize in Fig. 3 the mean values of each parameter obtained by both BSP and LSQ under different low b-values configurations. As observed, in both high-perfusion region (1st row) and low-perfusion region (2nd row), the mean of D^* decreases when reducing the number of low b-values, especially in high-perfusion region. The estimated D^* by BSP is closer to the ground-truth, compared to that by LSQ. The estimation of D or F was not affected by low b-values.

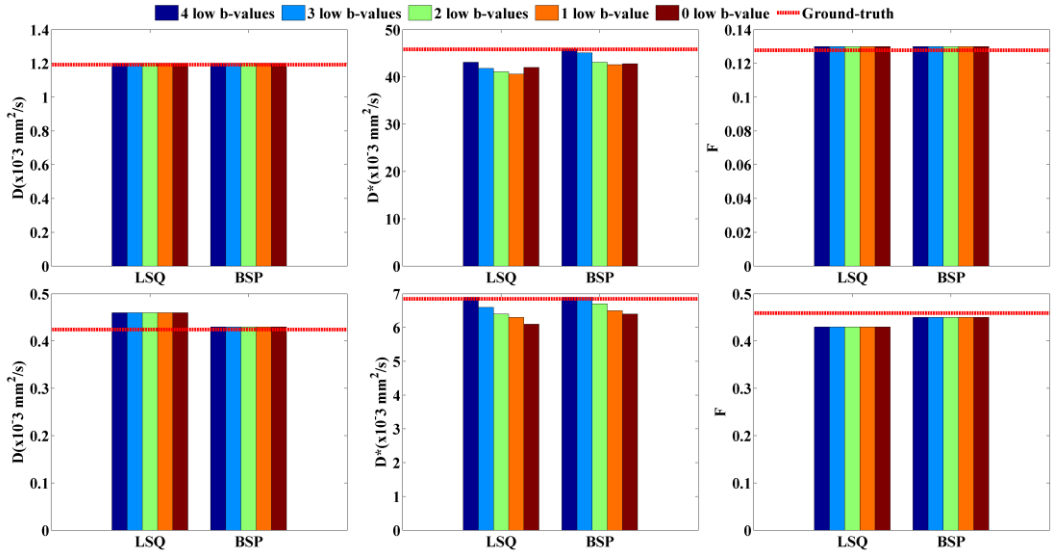

Fig. 3 Mean of IVIM parameters on simulation data with Gaussian noise. The first row represents the estimated results in high-perfusion regions, and the second row the results in low-perfusion regions.

To assess the impact of noise model on IVIM parameter estimation when using BSP method, two variants of BSP method with two noise models, namely BSP (Gaussian noise model) and BSP-Rician (Rician noise model) were compared. The results are given in Fig. 4. In both high perfusion region (Fig. 4(a)) and low perfusion region (Fig. 4(b)). Similar results are observed for the two BSP methods with the two noise models. Although at the low SNR (SNR=2), the RE generated by BSP-Ricain is slightly smaller than that produced by BSP, the results remain very close.

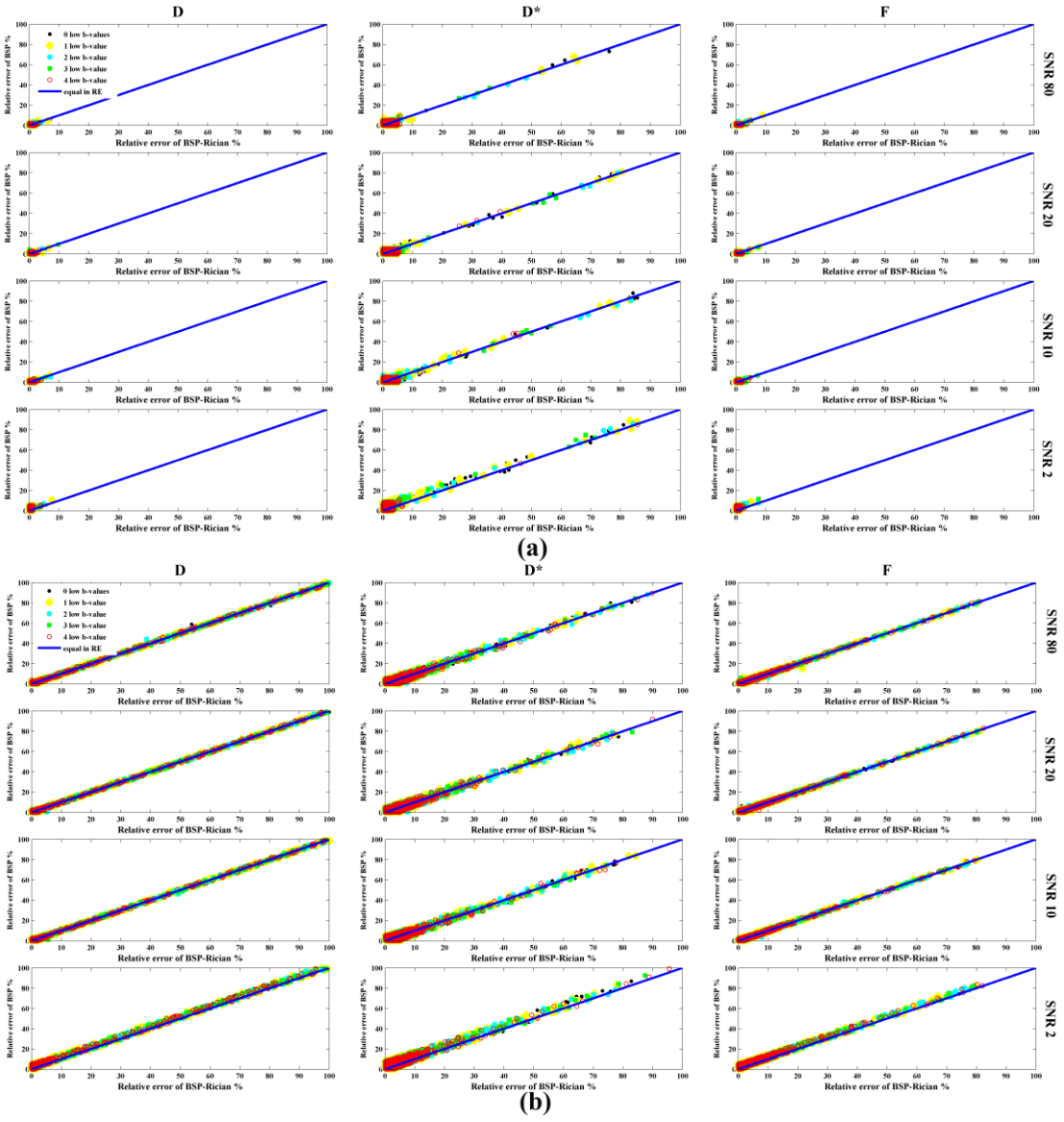

Fig. 4. Relative errors (REs) of the estimated IVIM parameters on simulation data with Rician noise. (a) REs in high-perfusion region. (b) REs in low-perfusion region. The coordinates of each point represent the REs of each voxel obtained using the two fitting methods, BSP and BSP-Rican, respectively.

The fitting results using different SNRs or different number of low b-values in heterogeneous regions are compared in Figs. 5. In Fig. 5(b), all the parameter maps were obtained using 4 low b-values. When the SNR was decreased, the parameter maps generated by the two fitting methods were heavily corrupted by noise, especially in perfusion-related parameter maps. BSP however generated smoother D^* and F maps than LSQ (red-boxed parameter maps), but induced at the same time information missing. When SNR is higher, the dependence on low b-values of BSP was also lower than that of LSQ in the heterogeneous region, as can be seen in Fig. 5(c). Indeed, when there is no low b-value, D^* maps estimated from LSQ or BSP are far away from ground truth (in particular loss of

higher D^* values). When passing from 4 low b-values to 1 low b-value, D^* map estimated from LSQ becomes sparser and loses higher D^* values while for BSP, the D^* maps change little and are slightly smoothed. In all cases, D map and F map vary little with the number of low b-values.

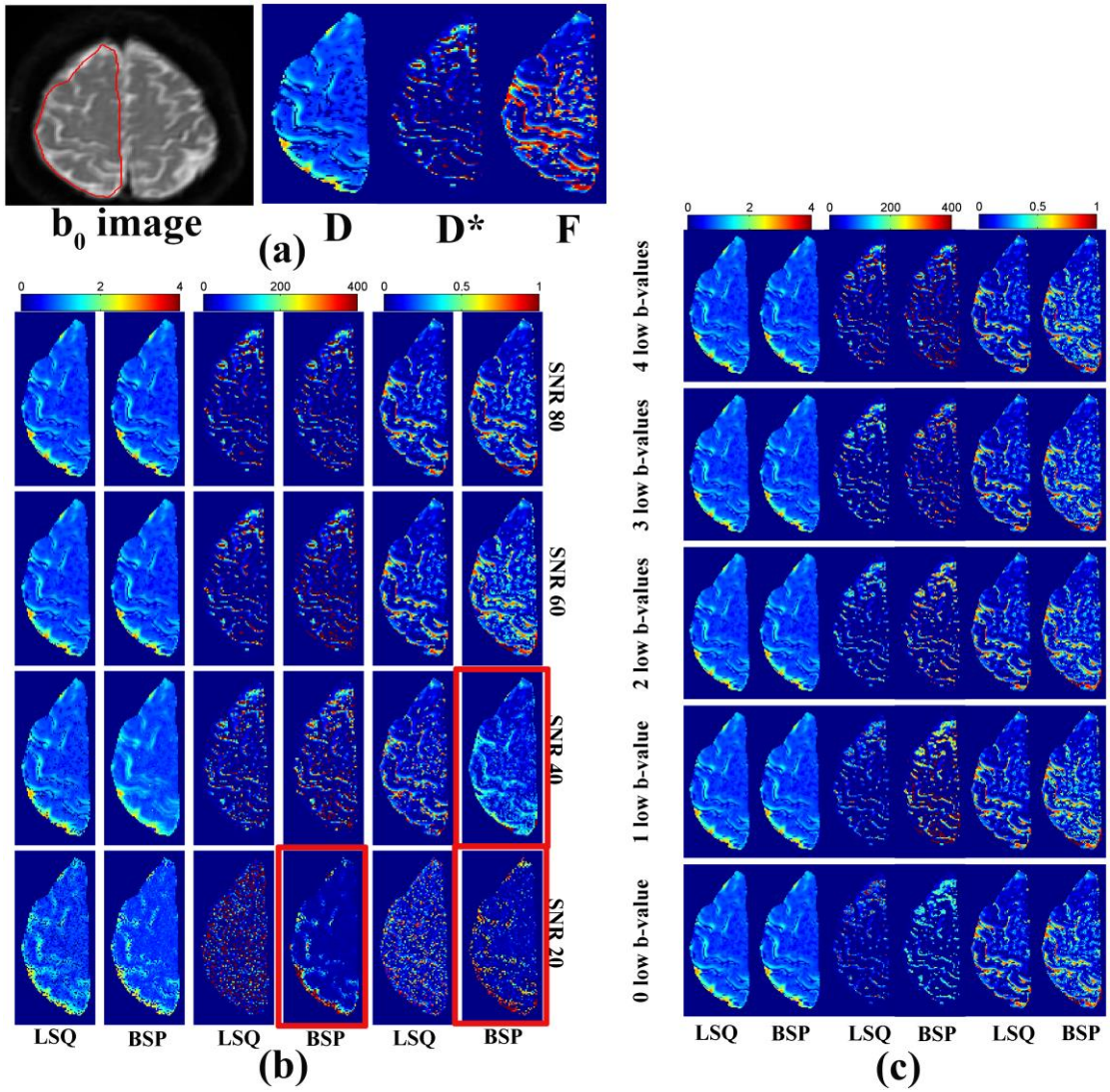

Fig. 5. Parameter maps of simulation data in heterogeneous region. (a) B_0 image marked with ROI of a healthy brain and the corresponding ground-truth parameter maps. (b) Parameter maps generated by LSQ and BSP using 4 low b-values. (c) An example of parameter maps at SNR 60 and with different number of low b-values. For (b) and (c), the first two columns represent D, the middle two columns D^* and the last two columns F. The red-boxed parameter maps show the situation where details are greatly smoothed out when using BSP.

The fitting results in homogeneous regions are shown in Fig. 6. Similar results to those in heterogeneous region were found. BSP generated cleaner parameter maps than LSQ. With the decreasing of SNR, D^* and F maps of both methods become more and more noisy, the rectangles tend

to disappear, and the values of some rectangles are altered (Fig. 6(a)). In contrast, *D* maps change relatively little although they also become somewhat noisier with the decreasing of SNR. The comparison of the effect of the number of low b-values on *D** estimation was shown in Fig. 6(b). For both LSQ and BSP, the estimated *D** in the subregion with high pseudo-diffusion coefficient (red rectangles) moves away from the ground-truth as the number of low b-values decreased, which is not the case for the blue and green areas (having relatively low pseudo-diffusion coefficient) that change little. Nevertheless, although noisier, the shape of the areas remains unchanged.

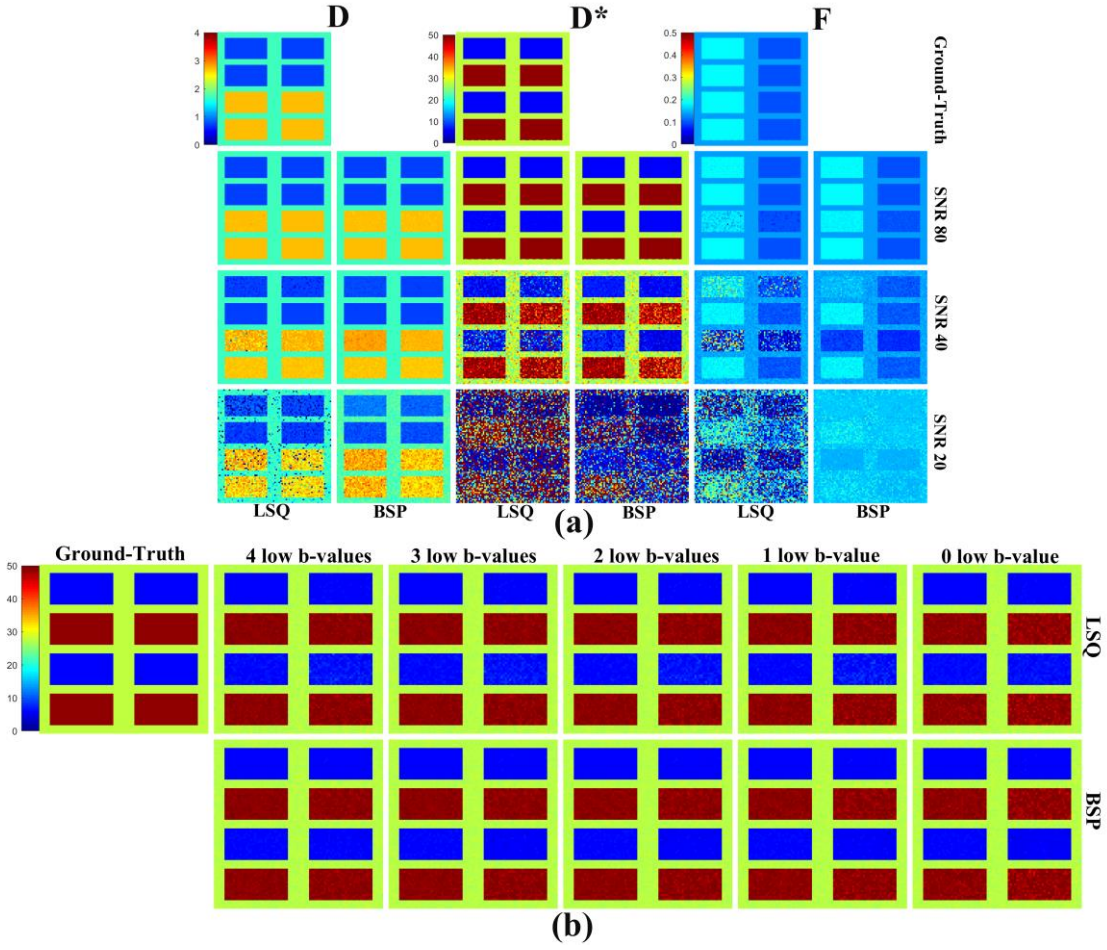

Fig. 6. Parameter maps of simulation data in homogenous regions. (a) Parameter maps generated by LSQ and BSP using 4 low b-values. (b) *D** maps at SNR 60 and with different number of low b-values. On the top row are given three ground-truth parameter maps, each of them contains 8 rectangles. In each parameter map of (a) and (b), different colors represent different homogenous areas. For example, in *D** map, the red rectangles represent the region with high *D**, the blue rectangles the region with low *D**, and the green areas the region with *D** whose value is the average of high and low parameter values.

3.2. In vivo images

The brain DW images marked with the tumor ROI of a meningioma are given in Fig. 7(a). The IVIM parameter maps of tumor ROI are shown in Fig. 7(b). BSP generates clearer parameter maps than LSQ. Results similar to simulation results are observed with respect to the effect of low b-values on parameter estimation. The estimation of *D* or *F* map of tumor region is insensitive to low b-values in comparison with *D** map of tumor region. The estimated *D** decreases with the reduction of the number of low b-values. The histograms of the obtained parameters are given in Fig. 7(c). The parameter distributions in the tumor region generated by BSP are more uniform than those by LSQ, which is reflected by the narrower IVIM parameter distribution of BSP with respect to LSQ. More outliers at the boundary of the constraints were generated by LSQ.

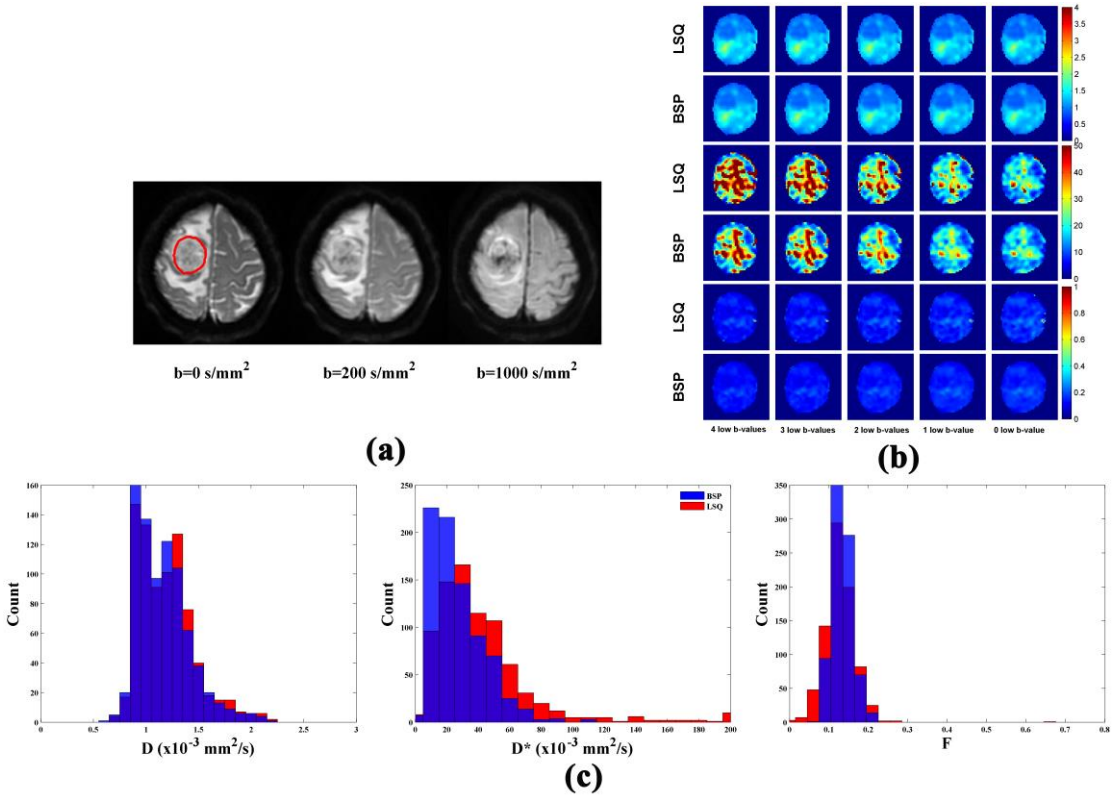

Fig. 7. (a) DW image marked with tumor ROI. (b) IVIM parameter maps of tumor ROI. The first two lines of (b) represent the parameter *D*, the middle two rows *D**, and the last two rows *F*. (c) histograms of parameters in (b) in the case of using 4 low b-values.

Bland-Altman analysis was performed to evaluate the intra-subject reproducibility of consecutive brain scans. The results on the tumor ROI in Fig. 7 are plotted in Fig. 8, where the mean biases (mean difference in the estimated parameter between two scans) are as follows. Mean bias in *D*: (LSQ,

BSP)=(+0.02 x10^{-3} mm^2/s, +0.01 x10^{-3} mm^2/s). Mean bias in *F*: (LSQ, BSP)=(+0.001, +0.001). Mean bias in *D**: (LSQ, BSP)=(+14.60 x10^{-3} mm^2/s, 10.32 x10^{-3} mm^2/s). The Bland-Altman repeatability coefficients (calculated as the half-length of the interval of the 95% confidence interval or limits of agreement) are the following. Repeatability coefficients for *D*: (LSQ, BSP)=(0.42 x10^{-3} mm^2/s, 0.15 x10^{-3} mm^2/s). Repeatability coefficients for *F*: (LSQ, BSP)=(0.26, 0.08). Repeatability coefficients for *D**: (LSQ, BSP)=(203.55 x10^{-3} mm^2/s, 67.48 x10^{-3} mm^2/s). Table 1 summarizes the details of the Bland-Altman analysis results over all the tumor ROIs. The mean values of bias over four brain tumor ROIs are the following. Mean bias in *D*: (LSQ, BSP)=(0.05 x10^{-3} mm^2/s, 0.03 x10^{-3} mm^2/s). Mean bias in *F*: (LSQ, BSP)=(0.03, 0.03). Mean bias in *D**: (LSQ, BSP)=(10.88 x10^{-3} mm^2/s, 3.26 x10^{-3} mm^2/s). The mean values of Bland-Altman repeatability coefficients are as follows. Mean repeatability coefficients for *D*: (LSQ, BSP)=(0.92 x10^{-3} mm^2/s, , 0.36 x10^{-3} mm^2/s). Mean repeatability coefficients for *F*: (LSQ, BSP)=(0.59, 0.24). Mean repeatability coefficients for *D**: (LSQ, BSP)=(365.56 x10^{-3} mm^2/s, 27.18 x10^{-3} mm^2/s). BSP exhibits better reproducibility with lower mean bias, narrower interval of limits of agreement and smaller mean Bland-Altman repeatability coefficient, compared to LSQ for all three IVIM parameters.

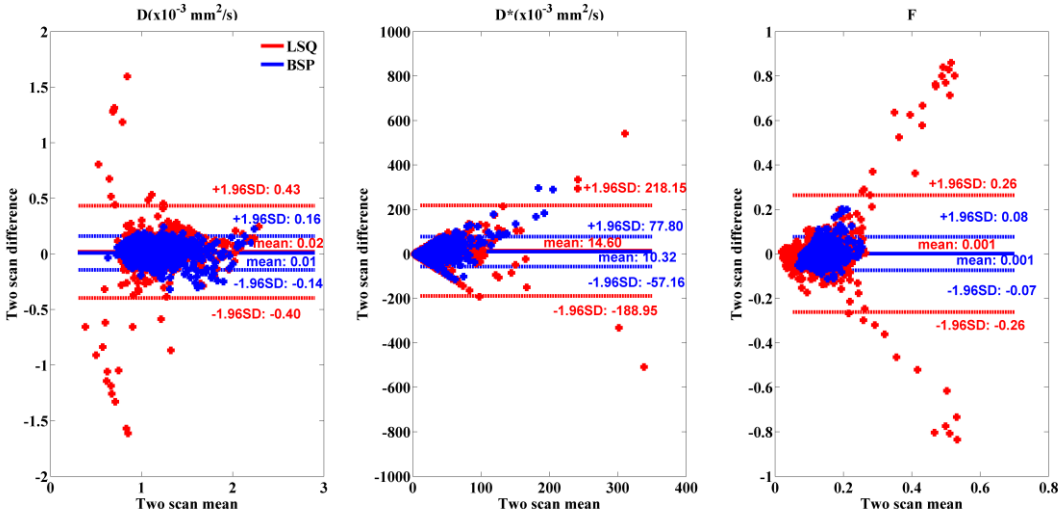

Fig. 8. Bland-Altman analysis for the tumor in Fig. 7. The plots show intra-subject reproducibility in the brain tumor region of two consecutive scans for both LSQ and BSP. The solid lines (red or blue) represent the mean difference in the estimated parameter between two scans, and the two paired dash (red or blue) lines represent the limits of agreement (95% confidence interval). Note that the blue BSP points are more tightly clustered, thus showing higher reproducibility and fewer outliers.

Table 1 Bland-Altman results with bias and limits of agreement (95% confidence interval) for in vivo brain tumor ROIs.

Subject	D ($\times 10^{-3}$ mm^2/s)		D* ($\times 10^{-3}$ mm^2/s)		F	
	LSQ	BSP	LSQ	BSP	LSQ	BSP
Mean bias						
1	0.02	0.01	14.60	10.32	0.001	0.001
2	-0.08	-0.06	-18	0.33	0.069	0.093
3	0.03	0.03	5.80	0.62	-0.01	-0.02
4	-0.08	-0.02	-5.11	1.78	0.04	-0.03
Mean[a]	0.05	0.03	10.88	3.26	0.03	0.03
P value[c]	0.24	0.30	0.23	0.58	0.45	0.48
Limits of agreement						
1	0.43	0.16	218.15	77.80	0.26	0.08
	-0.40	-0.14	-188.95	-57.16	-0.26	-0.07
2	0.94	0.15	515.89	10.14	0.76	0.31
	-1.10	-0.27	-551.88	-9.48	-0.63	-0.13
3	0.97	0.30	297.86	2.70	0.73	0.24
	-0.91	-0.23	-286.24	-1.47	-0.75	-0.30
4	1.22	0.89	427.65	31.11	0.72	0.35
	-1.39	-0.94	-437.87	-27.55	-0.64	-0.42
Mean[b]	0.92	0.36	365.56	27.18	0.59	0.24

"a": Mean value of bias across the four brain tumor ROIs. "b": Mean value of Bland-Altman repeatability coefficients across the four brain tumor ROIs. The Bland-Altman repeatability coefficient was calculated as the half-length of the interval of the limits of agreement. **"c": *P* values calculated by t-test to assess the significant difference of bias from zero.**

To further quantitatively analyze the effect of low b-values on parameter estimation, Fig. 9 plots the means and standard deviations of the parameters obtained over all the brain tumor ROIs. We observe similar results to the simulations. The estimation of D* was affected by the number of low b-values and especially for LSQ method. In contrast, the estimation of D or F was insensitive to low b-values.

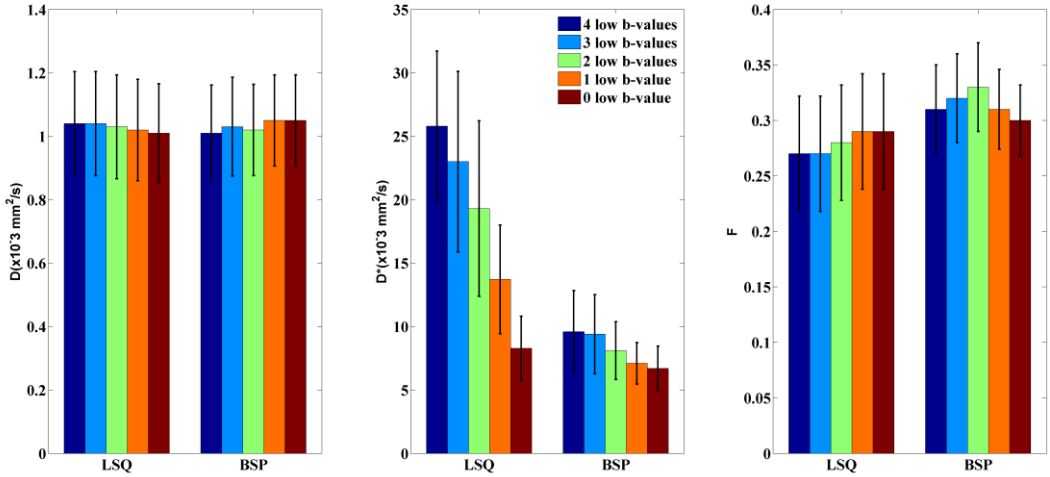

Fig. 9. The means and standard deviations of IVIM parameters of in vivo brains across all the tumor ROIs. The error bar indicates the standard deviation.

The differences in IVIM parameters between tumor and normal brain regions are given in Fig. 10 and Fig. 11. The comparison of parameter maps between the tumor in Fig. 7 and its corresponding normal region is shown in Fig. 10. All the parameter maps of the tumor region are clearly different from those of the normal region. It is visually easier to distinguish tumor from normal region in the results of BSP than in the results of LSQ, due to fewer outliers in the former. More details of IVIM parameter comparison between tumor and normal regions over all the subjects are summarized in Fig. 11. Obvious differences are observed between tumor and normal regions in parameters D ($p<0.05$) and F (especially F, $p<0.001$). BSP generated fewer outliers with respect to LSQ and distinguished better tumor from normal regions in parameter F.

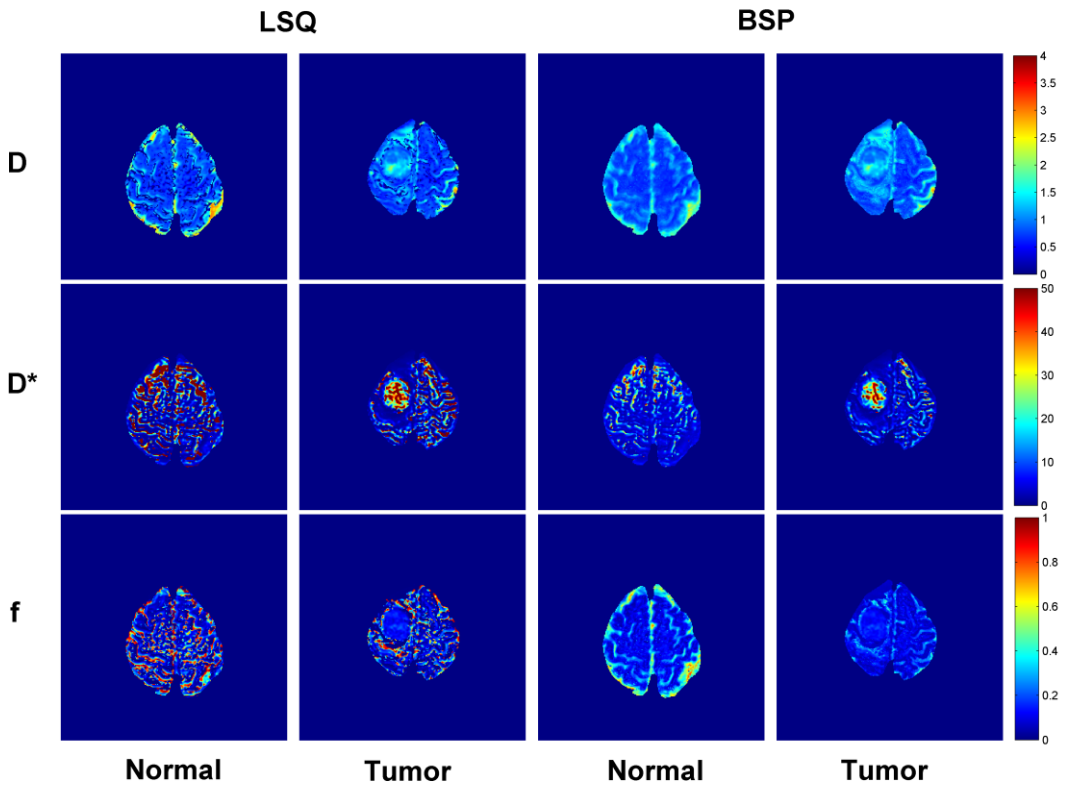

Fig. 10. Comparison of IVM parameter maps between the tumor in Fig. 7 and the corresponding normal region.

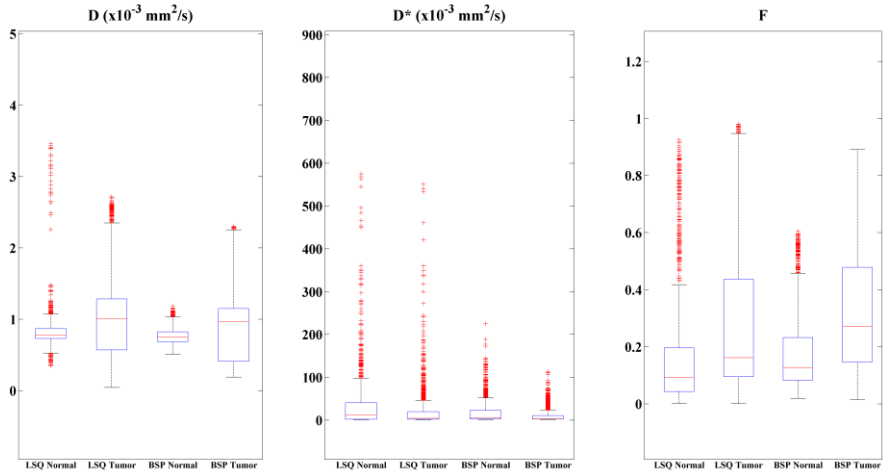

Fig. 11. Box-and-whisker plots summarizing results for all the tumor and normal ROIs.

4. Discussion

We have investigated IVIM parameter mapping of brain tumors using different low b-value configurations and fitting methods. It is generally recognized that perfusion information is very important in the application of IVIM to brain tumors. For example, the higher the tumor stage, the

higher the perfusion fraction. Poor accuracy of perfusion-related parameter estimation in previous studies is likely due to the deficiency of nonlinear least squares in solving the regression problem. LSQ aims by essence to obtain IVIM parameters by minimizing the residual between model and fitted signals. The more accurate the estimated parameter, the smaller the residual should be, but not vice versa. This is because different parameters of IVIM model play different role in signal attenuation. Pseudo-diffusion coefficient D^* is much greater than diffusion coefficient D. As a result, the contribution of perfusion component to the signal is weaker than that of diffusion component, due to the exponential IVIM model. That explains why in practice estimating accurately the weak contribution of D^* is difficult and any estimation bias of D^* will inevitably affect the estimation of the other perfusion-related parameter F. The RE map in simulations shows the superiority of Bayesian method: all the parameters obtained by BSP are closer to the ground-truth than those by LSQ, especially for the perfusion-related parameters. This is because BSP solves the regression problem in terms of probability, namely, it outputs the parameter by calculating the maximum posterior probability of signals instead of minimizing signal residual, thus the effect of the weak contribution of D^* to signals on parameter estimation is reduced.

To get more stable fitting results, the constraint on the range of parameter values was imposed in LSQ. We however observed an increase of the number of pixels undergoing outlying estimations at the boundary of the constraint. Since the uncertainty of LSQ parameter estimation is determined by the curvature of cost function of the minimization problem, this approach becomes inappropriate if the estimate is on a constraining boundary [19]. In contrast, BSP is strong enough to shrink outliers to the means of ROI, as shown in the in vivo experiment. Consequently, the histogram of IVIM parameters obtained by BSP is narrower than that obtained by LSQ due to the reduction of outlying estimations. That explains why BSP generated more uniform parameter maps compared to LSQ. Since BSP generated fewer outliers in parameter estimation, it differentiated better between brain tumor and normal regions.

However, whatever it was a heterogeneous region or a homogeneous region, when SNR was relatively low, BSP decreased and such decreasing was reflected by the disappearance of geometrical structures and appearance of quasi-homogeneous areas, though BSP generated fewer outliers with respect to LSQ. The latter however preserved better original heterogeneous parameter characteristics for high SNR and generated random noise-like parameter maps when SNR was low. This is

particularly obvious in D^* and F parameter maps for lower SNRs. That can be explained as follows. When SNR decreased, the choice of prior on parameter estimation was critical.[21] If the prior is far from the ground-truth of IVIM parameter distribution, the estimation of IVIM parameters will become inaccurate, which will be reflected for instance by the disappearance of information in the estimated parameter maps.

The obtained results showed that, besides fitting methods, low b-values also played a very important role in the parameter mapping of brain tumors. When low b-values were not used in IVIM parameter estimation, the pseudo-diffusion coefficient D^* of tumor tended to be underestimated. Similar finding was reported by Cohen et al. also in human livers. The difference is that liver is an organ that has relatively high pseudo-diffusion coefficients, and that, as a result, when low b-value acquisitions are absent, the contribution of perfusion component to the signal is near to zero. In this case, different values of D^* may generate close signal residuals, thus yielding underestimated D^*. However, previously-reported studies only considered the LSQ method and the impact of low b-values on D^* estimation in low-perfusion tissue was not addressed. The results in the present work clearly showed that the estimation of D^* by LSQ or BSP was dependent on low b-values, even in the low-perfusion region. Moreover, when using BSP, four low b-values were necessary for high-perfusion regions and three low b-values were in contrast enough for low-perfusion regions. When using LSQ, at least four low b-values were necessary for low-perfusion regions; in other cases, such as high-perfusion regions, even with four low b-values, D^* was underestimated. Hence, LSQ is more susceptible to low b-value than BSP, which was also verified in in vivo experiments.

Although BSP presents better performance than LSQ for parameter estimation, it requires more CPU execution time. This may become non-negligible if the amount of data is large.

Note that, with respect to the previous investigation about the effect of low b-values on parameter estimation,[34] which was focused on the human thigh having relatively higher pseudo-diffusion coefficients, the present work emphasized the accurate IVIM parameter estimation using Bayesian fitting and reduced number of low b-values for the human brain, which is considered as the low-perfusion tissue. The results showed that the number of low b-values is also very important for IVIM applications on low-perfusion tissue, and that Bayesian fitting allows clearly differentiating brain tumors from normal regions. Moreover, BSP requires less low b-values than LSQ, which also means shorter acquisition time.

Finally, the assumption on noise model should be taken into account in the use of the BSP method. In the present study, similar results were obtained when using BSP (Gaussian noise model) and BSP-Rician (Rician noise model) at higher SNRs. This is likely because Rician distribution tends toward Gaussian distribution at higher SNRs.[32, 33] When SNR is low, Rician distribution is closer to the actual noise model and the BSP-Rician model was more suitable for parameter estimation.

5. Conclusions

IVIM parameters allow clearly brain tumors to be differentiated from normal regions. Bayesian fitting yields robust IVIM parameter mapping with fewer outliers. Both BSP and LSQ fittings require enough number of low b-values for the accurate estimation of perfusion parameters of brain tumors, but BSP requires less low b-values than LSQ, which also represents shorter acquisition time.

Acknowledgements

This work was funded in part by the National Nature Science Foundations of China (Grant No. 61762019, 61661010, 81701654), the Funds for Talents of Guizhou University (No. 2013-33), the Nature Science Foundation of Guizhou province (Qiankehe J No.20152044, [2016]1096), and the Program PHC-Cai Yuanpei 2018 (N° 41400TC).

Conflict of Interest Statement

None declared.

References

[1] D. Le Bihan, E. Breton, D. Lallemand, P. Grenier, E. Cabanis, and M. Laval_Jeantet, MR imaging of Intravoxel Incoherent Motions: Application to Diffusion and Perfusion in Neurologic Disorders, Radiology **161**(2), 401–407 (1986).

[2] S. Bisdas, T.S. Koh, C. Roder, *et al.*, Intravoxel incoherent motion diffusion-weighted MR imaging of gliomas: Feasibility of the method and initial results, Neuroradiology **55**(10), 1189–1196 (2013).

[3] C. Federau, R. Meuli, K. O'Brien, P. Maeder, and P. Hagmann, Perfusion measurement in brain gliomas with intravoxel incoherent motion MRI, Am. J. Neuroradiol. **35**(2), 256–262 (2014).

[4] C. Federau, K. O'Brien, R. Meuli, P. Hagmann, and P. Maeder, Measuring brain perfusion with intravoxel incoherent motion (IVIM): Initial clinical experience, J. Magn. Reson. Imaging **39**(3), 624–632 (2014).

[5] A. Catanese, F. Malacario, L. Cirillo, *et al.*, Application of intravoxel incoherent motion (IVIM) magnetic resonance imaging in the evaluation of primitive brain tumours, Neuroradiol. J. **31**(1), 4–9 (2018).

[6] H.S. Kim, C.H. Suh, N. Kim, C.G. Choi, and S.J. Kim, Histogram analysis of intravoxel incoherent motion for differentiating recurrent tumor from treatment effect in patients with glioblastoma: Initial clinical experience, Am. J. Neuroradiol. **35**(3), 490–497 (2014).

[7] E.M. Meeus, J. Novak, S.B. Withey, N. Zarinabad, H. Dehghani, and A.C. Peet, Evaluation of intravoxel incoherent motion fitting methods in low-perfused tissue, J. Magn. Reson. Imaging **45**(5), 1325–1334 (2017).

[8] A. Andreou, D.M. Koh, D.J. Collins, *et al.*, Measurement reproducibility of perfusion fraction and pseudodiffusion coefficient derived by intravoxel incoherent motion diffusion-weighted MR imaging in normal liver and metastases, Eur. Radiol. **23**(2), 428–434 (2013).

[9] Z.X. Kuai, W.Y. Liu, Y.L. Zhang, and Y.M. Zhu, Generalization of intravoxel incoherent motion model by introducing the notion of continuous pseudodiffusion variable, Magn. Reson. Med. **76**(5), 1594–1603 (2016).

[10] C. Federau, P. Maeder, K. O'Brien, P. Browaeys, R. Meuli, and P. Hagmann, Quantitative Measurement of Brain Perfusion with Intravoxel Incoherent Motion MR Imaging, Radiology **265**(3), 874–881 (2012).

[11] C. Federau and K. O'Brien, Increased brain perfusion contrast with T2-prepared intravoxel incoherent motion (T2prep IVIM) MRI, NMR Biomed. **28**(1), 9–16 (2015).

[12] V.C. Keil, B. Mädler, G.H. Gielen, *et al.*, Intravoxel incoherent motion MRI in the brain: Impact of the fitting model on perfusion fraction and lesion differentiability, J. Magn. Reson. Imaging **46**(4), 1187–1199 (2017).

[13] P.T. While, A comparative simulation study of bayesian fitting approaches to intravoxel incoherent motion modeling in diffusion-weighted MRI, Magn. Reson. Med. **00**, 1–15 (2017).

[14] G.Y. Cho, L. Moy, J.L. Zhang, *et al.*, Comparison of fitting methods and b-value sampling strategies for intravoxel incoherent motion in breast cancer, Magn. Reson. Med. **74**(4), 1077–1085 (2015).

[15] H. Merisaari, P. Movahedi, I.M. Perez, *et al.*, Fitting methods for intravoxel incoherent motion imaging of prostate cancer on region of interest level: Repeatability and gleason score prediction, Magn. Reson. Med. **77**(3), 1249–1264 (2017).

[16] R. Fusco, M. Sansone, and A. Petrillo, A comparison of fitting algorithms for diffusion-weighted MRI data analysis using an intravoxel incoherent motion model, Magn. Reson. Mater. Physics, Biol. Med. **30**(2), 113–120 (2017).

[17] H.J. Park, Y.S. Sung, S.S. Lee, *et al.*, Intravoxel incoherent motion diffusion-weighted MRI of the abdomen: The effect of fitting algorithms on the accuracy and reliability of the parameters, J. Magn. Reson. Imaging **45**(6), 1637–1647 (2017).

[18] M. Freiman, J.M. Perez-Rossello, M.J. Callahan, *et al.*, Reliable estimation of incoherent motion parametric maps from diffusion-weighted MRI using fusion bootstrap moves, Med. Image Anal. **17**(3), 325–336 (2013).

[19] M.R. Orton, D.J. Collins, D.-M. Koh, and M.O. Leach, Improved intravoxel incoherent motion analysis of diffusion weighted imaging by data driven Bayesian modeling., Magn. Reson. Med. **71**(1), 411–20 (2014).

[20] G.R. Spinner, C. Von Deuster, K.C. Tezcan, C.T. Stoeck, and S. Kozerke, Bayesian intravoxel incoherent motion parameter mapping in the human heart, J. Cardiovasc. Magn. Reson. **19**(1), 1–14 (2017).

[21] O. Gustafsson, M. Montelius, G. Starck, and M. Ljungberg, Impact of prior distributions and central tendency measures on Bayesian intravoxel incoherent motion model fitting, Magn. Reson. Med. **00**, 1–10 (2017).

[22] A.D. Cohen, M.C. Schieke, M.D. Hohenwalter, and K.M. Schmainda, The effect of low b-values on the intravoxel incoherent motion derived pseudodiffusion parameter in liver, Magn. Reson. Med. **73**(1), 306–311 (2015).

[23] G. Gambarota, E. Hitti, B. Leporq, H. Saint-Jalmes, and O. Beuf, Eliminating the blood-flow confounding effect in intravoxel incoherent motion (IVIM) using the non-negative least square analysis in liver, Magn. Reson. Med. **77**(1), 310–317 (2017).

[24] A.M. Chow, D.S. Gao, S.J. Fan, *et al.*, Liver fibrosis: An intravoxel incoherent motion (IVIM) study, J. Magn. Reson. Imaging **36**(1), 159–167 (2012).

[25] S. Colagrande, F. Pasquinelli, L.N. Mazzoni, G. Belli, and G. Virgili, MR-diffusion weighted imaging of healthy liver parenchyma: Repeatability and reproducibility of apparent diffusion coefficient measurement, J. Magn. Reson. Imaging **31**(4), 912–920 (2010).

[26] R. van der Bel, O.J. Gurney-Champion, M. Froeling, E.S.G. Stroes, A.J. Nederveen, and C.T.P. Krediet, A tri-exponential model for intravoxel incoherent motion analysis of the human kidney: In silico and during pharmacological renal perfusion modulation, Eur. J. Radiol. **91**(March), 168–174 (2017).

[27] T. Finkenstaedt, M. Klarhoefer, C. Eberhardt, *et al.*, The IVIM signal in the healthy cerebral gray matter: A play of spherical and non-spherical components, Neuroimage **152**, 340–347 (2017).

[28] S. Bisdas and U. Klose, IVIM analysis of brain tumors: an investigation of the relaxation effects of CSF, blood, and tumor tissue on the estimated perfusion fraction, Magn. Reson. Mater. Physics, Biol. Med. **28**(4), 377–383 (2015).

[29] J. Sijbers, P. Scheunders, N. Bonnet, D. Van Dyck, and E. Raman, Quantification and improvement of the signal-to-noise ratio in a magnetic resonance image acquisition procedure, Magn. Reson. Imaging **14**(10), 1157–1163 (1996).

[30] M. Bertleff, S. Domsch, S. Weingärtner, *et al.*, Diffusion parameter mapping with the combined intravoxel incoherent motion and kurtosis model using artificial neural networks at 3 T, NMR Biomed. **30**(12), 1–11 (2017).

[31] A. Boss, B. Barth, L. Fili, *et al.*, Simultaneous multi-slice echo planar diffusion weighted imaging of the liver and the pancreas: Optimization of signal-to-noise ratio and acquisition time and application to intravoxel incoherent motion analysis, Eur. J. Radiol. **85**(11), 1948–1955 (2016).

[32] S. Walker- Samuel, M. Orton, L.D. McPhail, and S.P. Robinson, Robust estimation of the apparent diffusion coefficient (ADC) in heterogeneous solid tumors, Magn. Reson. Med. An Off. J. Int. Soc. Magn. Reson. Med. **62**(2), 420–429 (2009).

[33] H. Gudbjartsson and S. Patz, The Rician distribution of noisy MRI data, Magn. Reson. Med. **34**(6), 910–914 (1995).

[34] C. Ye, D. Xu, Y. Qin, *et al.*, Estimation of intravoxel incoherent motion parameters using low b-values, PLoS One **14**(2), 1–16 (2019).

Figure Captions

Fig. 2 Flowchart of BSP fitting.

Fig. 2. Relative errors (REs) of the estimated IVIM parameters on simulation data with Gaussian noise. (a) REs in high-perfusion region (b) REs in low-perfusion region. The coordinates of each point represent the RE of each voxel obtained using the two fitting methods.

Fig. 3 Mean of IVIM parameters on simulation data with Gaussian noise. The first row represents the estimated results in high-perfusion regions, and the second row the results in low-perfusion regions.

Fig. 4. Relative errors (REs) of the estimated IVIM parameters on simulation data with Rician noise. (a) REs in high-perfusion region. (b) REs in low-perfusion region. The coordinates of each point represent the REs of each voxel obtained using the two fitting methods, BSP and BSP-Rican, respectively.

Fig. 5. Parameter maps of simulation data in heterogeneous region. (a) B0 image marked with ROI of a healthy brain and the corresponding ground-truth parameter maps. (b) Parameter maps generated by LSQ and BSP using 4 low b-values. (c) An example of parameter maps at SNR 60 and with different number of low b-values. For (b) and (c), the first two columns represent D, the middle two columns D* and the last two columns F. The red-boxed parameter maps show the situation where details are greatly smoothed out when using BSP.

Fig. 6. Parameter maps of simulation data in homogenous regions. (a) Parameter maps generated by LSQ and BSP using 4 low b-values. (b) D* maps at SNR 60 and with different number of low b-values. On the top row are given three ground-truth parameter maps, each of them contains 8 rectangles. In each parameter map of (a) and (b), different colors represent different homogenous areas. For example, in D* map, the red rectangles represent the region with high D*, the blue rectangles the region with low D*, and the green areas the region with D* whose value is the average of high and low parameter values.

Fig. 7. (a) DW image marked with tumor ROI. (b) IVIM parameter maps of tumor ROI. The first two lines of (b) represent the parameter *D*, the middle two rows *D**, and the last two rows *F*. (c) histograms of parameters in (b) in the case of using 4 low b-values.

Fig. 8. Bland-Altman analysis for the tumor in Fig. 7. The plots show intra-subject reproducibility in the brain tumor region of two consecutive scans for both LSQ and BSP. The solid lines (red or blue) represent the mean difference in the estimated parameter between two scans, and the two paired dash (red or blue) lines represent the limits of agreement (95% confidence interval). Note that the blue BSP points are more tightly clustered, thus showing higher reproducibility and fewer outliers.

Fig. 9. The means and standard deviations of IVIM parameters of in vivo brains across all the tumor ROIs. The error bar indicates the standard deviation.

Fig. 10. Comparison of IVM parameter maps between the tumor in Fig. 7 and the corresponding normal region.

Fig. 11. Box-and-whisker plots summarizing results for all the tumor and normal ROIs.